Research Article | Vol. 27, No. 16 | 5 Aug 2019 | OPTICS EXPRESS 22127
Optics EXPRESS

Experimental all-optical relay-assisted FSO link with regeneration and forward scheme for ultra-short pulse transmission

NORHANIS AIDA MOHD NOR,[1,*] MATĚJ KOMANEC,[2] JAN BOHATA,[2] ZABIH GHASSEMLOOY,[3] MANAV R. BHATNAGAR,[4] AND STANISLAV ZVÁNOVEC[2]

[1]*Department of Science, Kulliyyah of Engineering, International Islamic University Malaysia, P.O. Box 10, 50728 Kuala Lumpur, Malaysia*
[2]*Department of Electromagnetic Field, Faculty of Electrical Engineering, Czech Technical University in Prague, Technicka 2, Prague 16627, Czech Republic*
[3]*Optical Communications Research Group, Faculty of Engineering and Environment, Northumbria University, Newcastle upon Tyne, NE1 8ST, UK*
[4]*Department of Electrical Engineering, Indian Institute of Technology Delhi, Hauz Khas, New Delhi 110016, India*
[*]*norhanis_aida@iium.edu.my*

Abstract: This paper presents experimental results for an all-optical free-space optical (FSO) relay-assisted system by employing an all-optical regenerate and forward (AORF) scheme in order to increase the transmission link span. The ultra-short pulse (i.e., 2 ps) regeneration technique based on Mamyshev method is adopted. We have developed a dedicated experimental test-bed composed of optical fiber components and FSO links to demonstrate the proposed scheme and evaluate its performance in terms of the Q-factor and bit error rate (BER) under turbulence regimes for both single and dual-hop network architectures. We show that, using the AORF a hundred times improvement in the BER performance is achieved compared to the amplify-and-forward scheme for a fixed signal-to-noise ratio under turbulence conditions.

1. Introduction

Free-space optical (FSO) communication technologies can offer similar capabilities as optical fiber communications and therefore can be considered as a promising candidate for the "last mile" access networks in the next generation broadband wireless communication networks [1,2]. This is mainly due to attractive features of the FSO technology including extremely wide bandwidth to support high transmission data rates, no licensing fee requirement, a high degree of security against eavesdropping at the physical level, low cost of installation and maintenance as well as immunity to the radio frequency induced electromagnetic interference [3,4]. Considering these advantages as well as the recent developments made in optoelectronic devices (i.e., improved energy efficiency, high-speed, compactness, etc.), the FSO technology is now being adopted in a number of applications including metro access networks, local-area network connectivity, long-haul systems, underwater communication networks, backup and disaster recovery situations [5]. For example, in [6] a 1.6 Tbps outdoor FSO system over a link span of 80 m based on the dense wavelength division multiplexing technique has been reported.

However, despite the advantages, the FSO link performance is degraded by the atmospheric conditions such as fog, rain, smog, snow and turbulence, which results in scattering and absorption of propagating optical signal, thus leading to attenuation, waveform distortion and phase wandering [7]. Even under a clear weather condition, propagating of optical wave-front will experience both intensity and phase fluctuations caused by the atmospheric turbulence, also

#367128 https://doi.org/10.1364/OE.27.022127
Journal © 2019 Received 13 May 2019; revised 3 Jul 2019; accepted 9 Jul 2019; published 22 Jul 2019

Optics EXPRESS

known as the scintillation, which ultimately results in the system performance degradation [8]. In order to mitigate the influence of atmospheric conditions and in particular turbulence, a number of mitigation schemes including diversity, coding, and adaptive threshold detection have been proposed. The latter offers an improved average bit error rate (BER) with low complexity [9]. In path diversity-based schemes, a number of nodes are used to deliver the information from the source to the destination node, i.e., the concept of relay-assisted FSO system [10, 11].

Most of the theoretical studies reported on the relay-assisted FSO systems under turbulence conditions [12–16] have considered the relay nodes using electrical-to-optical and optical-to-electrical conversion modules. Thus, there is the need for high-speed electronics and electro-optic devices, analog gain units and digital control modules, which significantly increases the link latency, complexity and implementation cost. Alternatively, FSO systems with all-optical relaying, i.e., amplify-and-forward (AF) using an erbium-doped fiber amplifier (EDFA), have been reported [17–20]. In [21], an all-optical AF dual-hop FSO system leveraging a 4-pulse position modulation (4-PPM) and operating at the wavelength (λ) of 1550 nm over Gamma-Gamma turbulence channel was reported. However, almost all the works reported on this topic are theoretical in nature with limited or no experimental verifications. Moreover, investigation of the all-optical based regeneration and re-shaping of ultra-short (i.e., higher bit rates) pulses in FSO systems has not been reported yet in the literature.

In [22], we experimentally verified the performance of an all-optical dual-hop 10 Gbps FSO link by employing all-optical switching at the re-transmission point under the turbulence condition. In [23] and [24], we also experimentally investigated an all-optical triple-hop AF FSO relay-assisted system over several turbulence channel configurations and conditions and provided mathematical frameworks for the end-to-end signal-to-noise ratio (SNR) and the BER performance for the N-hop relay-assisted AF FSO system. Even though the AF is the simplest relaying scheme, the optical amplifier boosts both the signal and noise at each relay, therefore imposing a limit on the number of relays that can be employed over a long FSO span due to reduced SNR.

To overcome this problem, an all-optical regenerate-and-forward (AORF) technique is introduced in this paper, which can be adopted at each relay in order to increase the transmission link span as part of the last miles access wireless networks in urban areas. In [18], an all-optical 2R Mamyshev-based regenerator for FSO communications was theoretically analysed to mitigate accumulation of the background noise. It was shown that, at the BER of 10^{-5} and a transmit power of 500 mW, bit rate of 10 Gbps, wavelength of 1550 nm, bandpass filter (BPF) with 80 GHz bandwidth and 36 m long nonlinear optical fiber with nonlinearity of 1100 $W^{-1}km^{-1}$, the maximum transmission span was increased from 1.7 km to 2.6 km and 4.5 km for AF and AORF dual-hop relaying-based systems, respectively compared to the direct transmission based system. However, in [18], only the background noise was considered as the limiting factor, and the effect of atmospheric turbulence was neglected. Furthermore, in real applications a nonlinear optical fiber with such a high nonlinearity fabricated using chalcogenide or bismuth glass, normally has $>$ 1 dB/m of attenuation at 1550 nm, providing almost 40 dB of loss in the proposed AORF system, thus severely degrading the BER. Moreover, the AORF scheme for FSO links employing ultra-short pulses for high transmission data rates has not been experimentally investigated yet.

Therefore, the main aim of this paper is to experimentally verify and evaluate the concept of all-optical 2R regeneration (i.e., re-amplification and re-shaping) based on Mamyshev regeneration scheme as part of the FSO relay network in urban environments. As a proof of concept, the proposed scheme employs a return-to-zero (RZ) data format with a picosecond pulse duration, i.e., 2 ps full width at half maximum (FWHM). We also compare the performance of multi-hop AORF with AF-based FSO transmission under several turbulence regimes.

The remainder of this paper is organized as follows: Section 2 provides a detailed description of the concept of Mamyshev regeneration technique, short pulses setting and the pulse reconstruction

method. In section 3, we present the experimental setup and the corresponding FSO performance analyses. Also, measured results from AORF and AF schemes are compared. Lastly, concluding remarks are highlighted in Section 4.

2. Pulse reconstruction at the relay node

2.1. SPM-based AORF relaying concept

The relaying proposed in this paper is described as self-phase modulation (SPM)-based AORF relaying system, commonly referred as a Mamyshev regenerator [25]. It consists of three main components of EDFA, highly nonlinear fiber (HNLF) and BPF with a center wavelength with an offset to the original signal wavelength. For a Gaussian pulse transmitted through HNLF, the average spectral broadening is given by [25]:

$$\triangle\omega_{SPM} = \triangle\omega_0(2\pi/\lambda)n_2 I_p L, \tag{1}$$

where $(\triangle\omega_0 \sim 1/\tau)$ is the initial bandwidth of the signal pulse, τ is pulsewidth, λ is the wavelength, L is HNLF length, n_2 is the nonlinear refractive index of the HNLF and I_p is optical intensity of the signal pulse.

Following propagating through the HNLF, the signal pulses are applied to a BPF, whose center frequency ω_f is shifted with respect to the input signal carrier frequency by $\triangle\omega_{shift}$. Depending on the degree of spectral broadening, the BPF center frequency and its bandwidth $\triangle\ \omega_f$ only part of the SPM-broadened spectrum passes through BPF and the rest is suppressed. In the case, where I_p is significantly higher compared to the critical pulse intensity $I_{cr}(I_p \gg I_{cr})$, the pulse spectrum broadens extensively, while $\omega_{SPM}/2 \geq \triangle\omega_{shift}$ and the intensity of the output pulse I_{out} is independent of I_p. Therefore, this results in a nonlinear transfer function for the regenerator, which consequently improves the SNR by the way of reducing the noise. A pulse transfer function for the regenerator can be defined in terms of the output and input pulse intensities as given by [25]:

$$I_{out} = \begin{cases} 0 & if \quad I_p < I_{cr} \\ I_c & if \quad I_p > I_{cr} \end{cases} \tag{2}$$

where I_c is the constant output pulse intensity. I_{cr} can be adjusted to provide a trade-off between reducing the noise and suppressing amplitude fluctuations for binary "0" and "1", respectively and is defined as:

$$I_{cr} = \frac{2\triangle\omega_{shift}}{\triangle\omega_0(2\pi/\lambda)n_2 L}. \tag{3}$$

2.2. Regenerator configuration and optimization

The schematic block diagram of the proposed AORF configuration is depicted in Fig. 1. For the purpose of ultra-short pulse generation, a wavelength-tunable mode-locked laser (MLL) with a center wavelength of 1547 nm (MLL, u2t photonics) is used to produce Gaussian-shaped pulses with FWHM of 2.2 ps (i.e., 10 % duty cycle) for high transmission data rates. The laser signal propagating through a single mode fiber (SMF) is amplified using a low noise EDFA (Keopsys KPS-BT2-C-10-LN-SA) prior to being launched into a 2.2 m long FSO channel (i.e., FSO 1) via a variable optical attenuator and a combination of gradient-index (GRIN, Thorlabs 50-1550A-APC) and plano-convex (PC, Thorlabs LA1509-C) lenses. At the other side of the FSO channel, the same combination of PC and GRIN lenses is used to couple the optical signal into a SMF. Note that, this configuration is adopted for both AF and AORF relay nodes. In AORF-based relay, the signal is once again amplified (Keopsys CEFA-C-PB-30) and then launched into the all-optical 2R regenerator based on Mamyshev principle [25,26], where a 500 m

long HNLF with 0.88 dB/km of attenuation is used to broaden signal spectrum via SPM. Note that, HNLF has a zero-dispersion at 1556 nm with a dispersion slope and a nonlinear coefficient of 0.019 ps/nm·km and 11.35 $W^{-1}km^{-1}$, respectively. A tunable optical BPF (Santec OTF-950) with the off-set wavelength is used to produce the spectrally broadened signal with suppressed noise. For AF-based relay, the optical signal is only amplified prior to re-transmission, see Fig. 1.

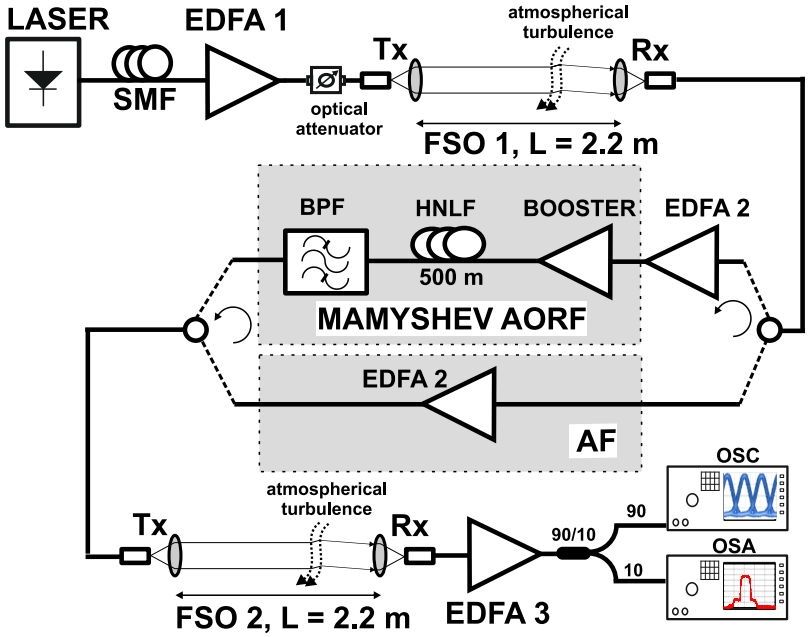

Fig. 1. Block diagram of the proposed system.

The output signal from the relay node is transmitted over a second FSO channel (i.e., FSO 2) with the identical setup as FSO 1. The optical signal is then captured using a combination of lenses followed by amplification (i.e., EDFA 3). A 90/10 power coupler is used for monitoring of the link performance (i.e., the eye diagram and the Q-factor) using a digital oscilloscope (OSC, 10 GHz Agilent 86100C) and an optical spectrum analyzer (OSA, Yokogawa AQ-6370). Fig. 2 displays an experimental test-bed for the proposed system. Note that, the received signal at the input of the EDFA 3 is defined as:

$$y_0 = sh_{eq} + n_{eq}, \tag{4}$$

where s is the transmitted signal and $h_{eq} = G_1 h_1 h_2$ is equivalent channel gain, G_1 is the relay gain, and $h_{1,2}$ channels 1 and 2 gains, n_{eq} is equivalent additive white Gaussian noise with zero mean and variance representing the ambient light σ_n^2 and the amplified spontaneous emission noise σ_a^2 of the EDFA.

For the FSO links, the turbulence was generated using fan heaters positioned along the atmospheric chamber i.e., creating a temperature gradient. A number of temperature sensors (in this case 20) positioned along the chamber were used to measure the temperature profile every 4 second. Note, with no turbulence, the temperature within the channel was kept at the room temperature. Based on the sensor outputs we characterized turbulence via the refractive index structure parameter (in detail described in [21]), which is given by [1, 11]:

$$C_n^2 = \left(86 \cdot 10^{-16} \frac{P}{T^2}\right)^2 C_T^2, \tag{5}$$

Optics EXPRESS

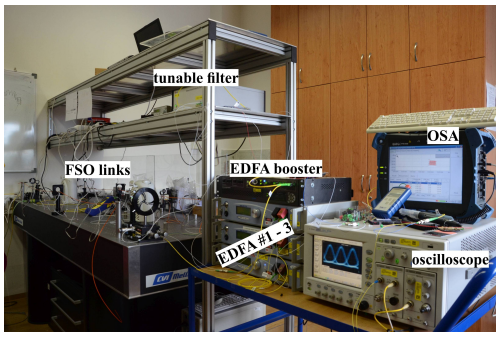

Fig. 2. Experimental test-bed for the triple-hop FSO system.

where P is atmospheric pressure in millibar, T is the absolute temperature in Kelvin, C_T^2 is the temperature structure constant, which is related to the universal 2/3 power law of temperature. Another important parameter that is commonly used to determine the turbulence regime is Rytov variance σ_R^2, which is defined as [1, 11]:

$$\sigma_R^2 = 1.23\, C_n^2\, k^{7/6}\, L_D^{11/6} \tag{6}$$

where $k = 2\pi/\lambda$ is the wave number (or the propagation constant), and L_D is the propagation distance. The main system parameters are given in Tab. 2.2.

At first, we verify the MLL pulse FWHM when amplified by EDFA 1 using an optical auto-correlator what is displayed in Fig. 3. Note that, the measured pulse FWHM is 2.2 ps. To optimize AORF with respect to the SPM, we have developed a simulation model with elements corresponding to the parameters of real components and devices. The maximum optical power is set to 20 dBm, which is typically maximal power used in all fiber/FSO systems. We evaluate the following three variables of EDFA output power (i.e., not including amplified spontaneous emission - ASE), the BPF center wavelength and its FWHM. Based on the simulation, the EDFA 2 output power is optimized to 16 dBm, which is adopted for the experimental investigation. Figs. 4(a) and 4(b) show the simulated and measured spectra at the output of HNLF used in AORF for a range of EDFA 2 output power levels. The results show a good match at the wavelength range of $1535 < \lambda < 1550$ nm with the profile at longer wavelengths mainly being affected by the ASE from EDFA.

To regenerate the input signal for the binary "1s", we set the BPF central wavelength at 1551 nm where the SPM broadened spectra experiences a higher SNR (i.e., high intensity and minimum noise). The original signal spectrum, spectrum broadened by SPM and the final output filtered AORF spectrum are depicted in Fig. 5.

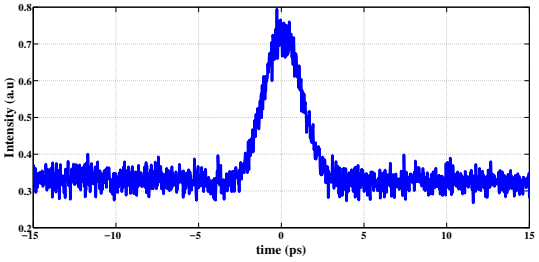

Fig. 3. MLL pulsed output at 1547 nm amplified to 9 dBm by EDFA 1.

Table 1. Main Parameters Used in Experiment.

	Parameter	Value
Transmitter	Pulse type	RZ
	Repetition rate	10 GHz
	Laser type	Mode-locked
	Central wavelength	1547 nm
	Output average power	-17.2 dBm
Collimators	GRIN-lens aperture	0.18 cm
	GRIN-lens working distance	1.5 cm
	PC-lens clear aperture	2.54 cm
	PC-lens focal distance	10.0 cm
FSO channels	Length	2.2 m
	Loss	16.0 dB
EDFA - preamp.	Max. output power	10 dBm
	Noise figure	< 5.0 dB
EDFA - booster	Max. output power	30 dBm
	Noise figure	< 5.5 dB
HNLF	Length	500 m
	Attenuation	0.88 dB/km
	Nonlinear coefficient	11.35 $W^{-1}km^{-1}$
Optical BPF	Central wavelength	1551 nm
	Bandwidth	3 nm
	Insertion loss	4 dB

3. Performance comparison of AORF FSO with AF

This section discusses the measured BER results for the dual-hop AORF systems and compares them with the AF system for various turbulence regimes. The measured data are compared with the simulation results in order to provide validation. In addition, we provide measured eye diagrams to confirm the achieved results.

3.1. Performance verification of AORF single FSO link

In order to compare signal degradation and regeneration, the measured optical pulses from the auto-correlator at the outputs of FSO link 1 and Mamyshev AORF-based relay node are illustrated in Figs. 6(a) and 6(b).

It can be seen that, following regeneration, the SNR is significantly improved by way of reducing

Optics EXPRESS

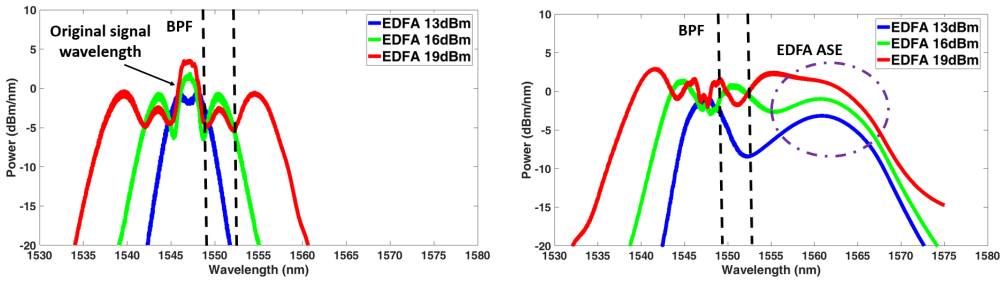

(a) (b)

Fig. 4. AORF HNLF output spectrum for a range of EDFA output power for: (a) simulation, and (b) measured.

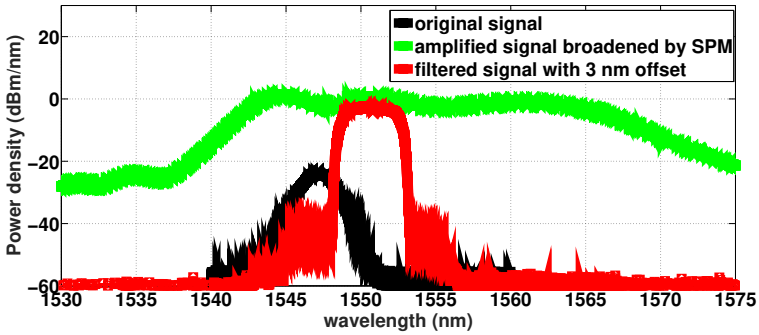

Fig. 5. Original MLL spectrum, SPM-broadened spectrum for EDFA at 16 dBm and the BPF central λ of 1551 nm.

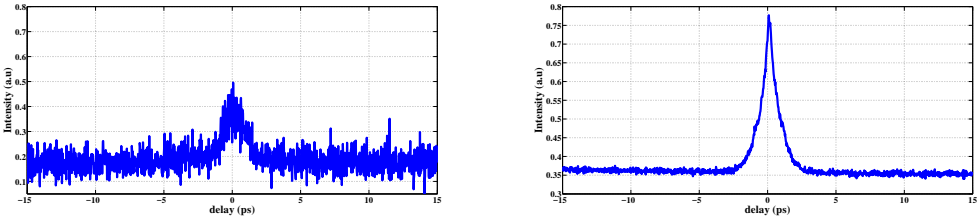

(a) (b)

Fig. 6. Measured pulse from autocorrelator at the output of: (a) FSO 1, and (b) AORF Mamyshev regeneration.

the noise level. Note, in order to implement the regeneration of the pulse the offset filtering relative to the carrier wavelength is mandatory. Under offset filtering, the binary "1" with a higher power level induce significant spectral broadening (i.e., spreading into the spectral transmission window of the spectral slicing filter), whereas bits "0" with lower power levels experience negligible or no spectral broadening, thus are "blocked". Therefore, intensity discrimination is achieved for the regenerator, and consequently, with improved extinction ratio [25, 26].

3.2. Dual-hop FSO link

In this section, we outline measured results for the proposed system with a total FSO link span of 4.4 m. Figure 7 depicts the measured BER as a function of SNR for the AF-based dual-hop FSO relay-assisted scheme with and without turbulence. Also shown for comparison is the predicted BER for the proposed link using the derivation in [23]. As expected, stronger turbulence results in higher SNR penalties. For instance, at a target BER of 10^{-3}, the SNR penalties are ~3.1 dB, ~8.2 dB, and ~9.4 dB for C_n^2 of $1.6{\cdot}10^{-11}$ $m^{-2/3}$, $6.8{\cdot}10^{-10}$ $m^{-2/3}$, and $1.9{\cdot}10^{-9}$ $m^{-2/3}$, respectively for the measured data compared to the link with no turbulence. The corresponding Rytov variance σ_R^2 values for mentioned C_n^2 are $3.48{\cdot}10^{-3}$, 0.148, and 0.414, respectively for L = 2.2 m. For typical last mile access with a distance of 500 m, C_n^2 will be $9.65{\cdot}10^{-15}$ $m^{-2/3}$, $4.11{\cdot}10^{-13}$ $m^{-2/3}$ and $1.15{\cdot}10^{-12}$ $m^{-2/3}$ corresponding to our initial σ_R^2 of $3.48{\cdot}10^{-3}$, 0.148, and 0.414, respectively.

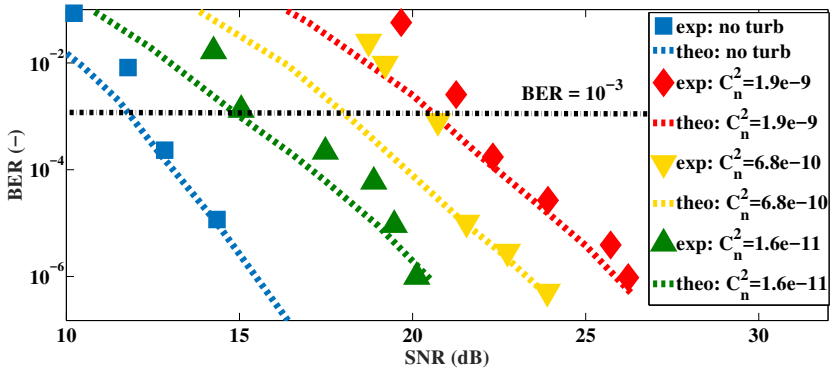

Fig. 7. BER vs. the optical SNR for the FSO dual-hop with AF relaying based system for a range of turbulence regimes.

A similar measurement is then carried out comparing the measured and theoretical BER as a function of the SNR for the dual-hop FSO using AORF (depicted in Fig. 8) under the three aforementioned turbulence regimes. The plots demonstrate that, under stronger turbulence regimes the propagating optical wavefront experiences much higher levels of intensity and phase fluctuations, thus leading to higher SNR penalties (i.e., increased BER) compared to the case with no turbulence. The slight mismatch between the theoretical and experimental results above the BER of 10^{-3} is caused by significantly decreased SNR in the experimental setup. In case of such BER levels, results are dominated by additive noise, which also includes ASE from EDFA.

Next, Fig. 9 illustrates a clear comparison of the measured BER performance against the optical SNR for AORF and AF dual-hop FSO relaying systems without and with turbulence. Results show that with AORF the BER performance has significantly improved compared to the AF (i.e., reduced BER by 10^1 to 10^3). E.g., at a target BER of 10^{-3} while using AF the power penalties are ~4 dB, ~2 dB, ~5 dB and ~3 dB for no turbulence, and C_n^2 of $1.9{\cdot}10^{-9}$ $m^{-2/3}$, $6.8{\cdot}10^{-10}$ $m^{-2/3}$, and $1.6{\cdot}10^{-11}$ $m^{-2/3}$, respectively compared to the AORF. This significant improvement is due to Mamyshev regenerator capability in removing the unwanted noise, and boosting the signal using the OA (i.e., higher SNR). Note that, the turbulence levels can be scaled (i.e., recalculated) for real outdoor link with much longer transmission spans by using Rytov variance [7]. As an example, for a 500 m long FSO link the corresponding C_n^2 are $7.65{\cdot}10^{-16}$ $m^{-2/3}$, $3.25{\cdot}10^{-14}$ $m^{-2/3}$ and $9.09{\cdot}10^{-14}$ $m^{-2/3}$.

Finally, we investigated different turbulence configurations along the dual-hop FSO link: (i) the FSO 1 with no turbulence and the FSO 2 with turbulence (i.e., $C_n^2 = 7.5{\cdot}10^{-10}$ $m^{-2/3}$); and (ii) the FSO 1 with turbulence (i.e., $C_n^2 = 7.5{\cdot}10^{-10}$ $m^{-2/3}$) and the FSO 2 with no turbulence. The

Optics EXPRESS

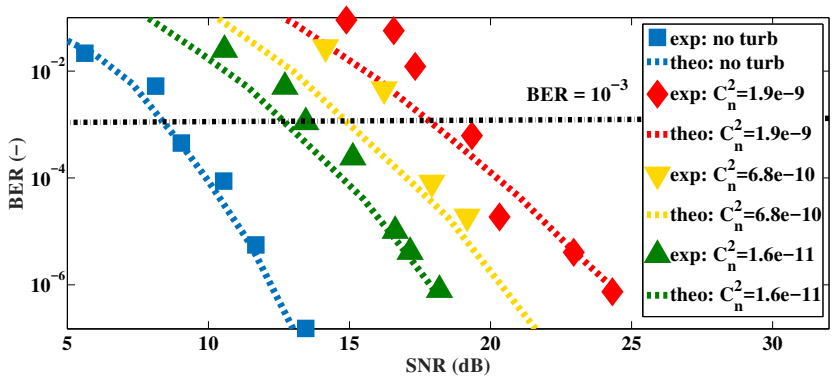

Fig. 8. BER vs. the optical SNR for the FSO dual-hop with AORF for a range of turbulence regimes.

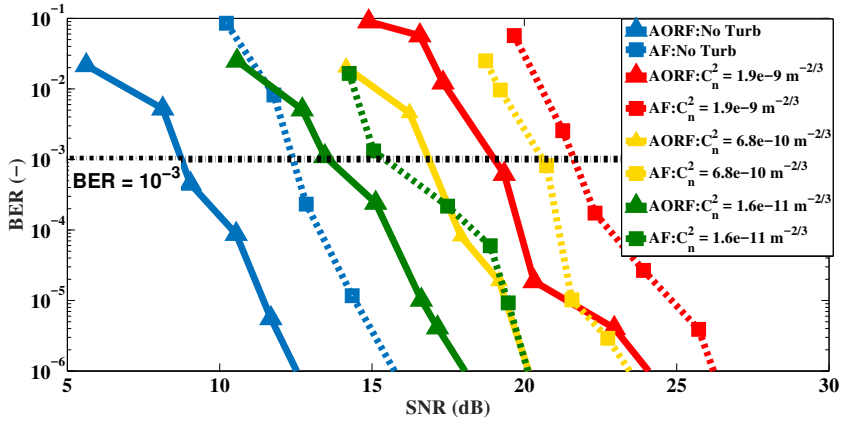

Fig. 9. BER vs. the optical SNR for the FSO dual-hop link with AORF and AF for a range of turbulence regimes.

predicted and measured BER as a function of the SNR for the above cases are depicted in Fig. 10. Results show that, for the measured case and for the FSO link 2 under atmospheric turbulence i.e., $C_n^2 = 7.5{\cdot}10^{-10}\,\mathrm{m}^{-2/3}$, the relay-based system experiences severe performance degradation comparable to the case with FSO link 1 under turbulence, i.e., the BER is increased from $7{\cdot}10^{-5}$ to $2{\cdot}10^{-2}$ at a SNR of 18 dB for the AF scheme. However, this can be greatly compensated by using AORF where the BER is reduced to 10^{-6} and $5{\cdot}10^{-4}$, respectively. This exceptional BER performance of the AORF relaying scheme is due to the usage of Mamyshev 2R regenerator where the unwanted noise is reduced significantly. Note that, there is a good match between the measured and predicted plots. The measured eye diagrams using the OSC for the dual-hop FSO link employing both AF and AORF schemes are shown in Fig. 11, which validates the measured BERs.

As can be clearly seen, for the high turbulence level (C_n^2 of $1.9{\cdot}10^{-9}\,\mathrm{m}^{-2/3}$) the eye diagrams are significantly closed with lower values of Q-factor (1.4 and 3.6 for AF and AORF, respectively) compared to the cases with no turbulence or lower levels of turbulence. Note, for the AORF link with no turbulence and with strong turbulence the Q-factor values are higher by 15 % and 54 %, respectively compared to the link with only AF.

Optics EXPRESS

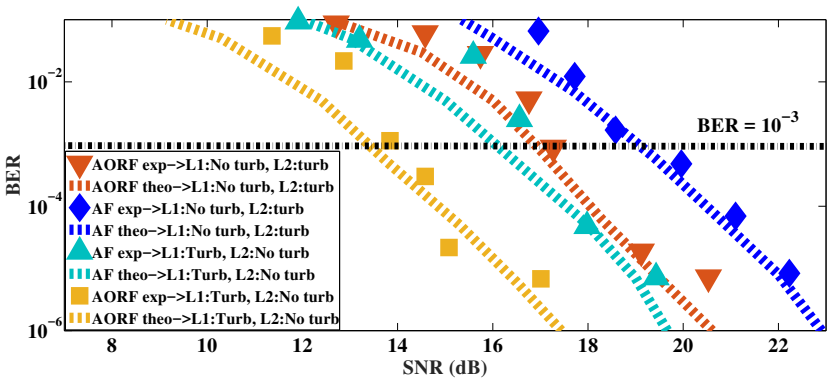

Fig. 10. BER against the SNR for AORF and AF based dual-hop FSO link with turbulence.

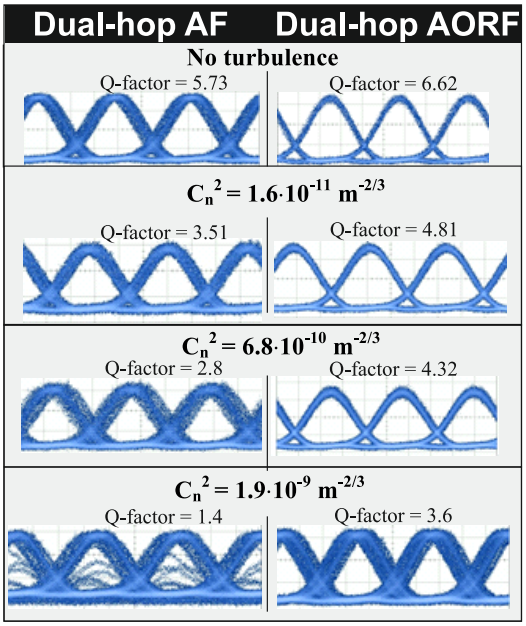

Fig. 11. Measured eye-diagrams for dual-hop FSO link with AF and AORF with and without turbulence.

4. Conclusions

In this paper, we reported an all-optical regeneration scheme for ultra-short pulses (~2 ps) based dual-hop FSO relay-assisted schemes for high transmission data rates. We assessed the proposed system performances in terms of the Q-factor and the BER for both AF and AORF-based schemes by exposing the FSO links to atmospherical turbulence. Results demonstrated a good agreement between the theoretical simulations and measurements, particularly at relatively high SNRs. It was shown, based on the experimental results, that the AORF-based scheme outperforms AF schemes by reducing BER by 10^1 to 10^3. Particularly, at a target BER of 10^{-3}, the SNR gains of ~4 dB, ~2 dB, ~5 B, and ~3 dB were achieved for low turbulence, C_n^2 of $1.9{\cdot}10^{-9}$ $m^{-2/3}$, $6.8{\cdot}10^{-10}$ $m^{-2/3}$, $1.6{\cdot}10^{-11}$ $m^{-2/3}$, respectively when using AORF compared to AF scheme. This impressive performance of AORF-based scheme has been achieved due to capability of the

Optics EXPRESS

system to remove accumulation of the background noise at the relay before re-transmission.

Funding

Grant Agency of the CTU in Prague (SGS17/182/OHK3/3T/13); MEYS INTERCOST project Traffic (LTC18008).

References

1. Z. Ghassemlooy, W. Popoola, and S. Rajbhandari, *Optical wireless communications: System and channel modelling with MATLAB* (CRC Press Taylor and Francis Group, 2013), I ed.
2. M. A. Khalighi and M. Uysal, "Survey on free space optical communication: A communication theory perspective," IEEE Commun. Surv. Tut. **16**, 2231–2258 (2014).
3. A. Paraskevopoulos, J. Vučić, S. Voß, R. Swoboda, and K. Langer, "Optical wireless communication systems in the Mb/s to Gb/s range, suitable for industrial applications," IEEE/ASME Trans. Mechatronics **15**, 541–547 (2010).
4. M. Z. Chowdhury, M. T. Hossan, A. Islam, and Y. M. Jang, "A comparative survey of optical wireless technologies: Architectures and applications," IEEE Access **6**, 9819–9840 (2018).
5. M. Uysal, C. Capsoni, Z. Ghassemlooy, A. Boucouvalas, and E. Udvary, *Optical wireless communications: An emerging technology* (Springer, 2016).
6. G. Parca, A. Shahpari, V. Carrozzo, G. M. T. Beleffi, and A. L. J. Teixeira, "Optical wireless transmission at 1.6-Tbit/s (16x100 Gbit/s) for next-generation convergent urban infrastructures," Opt. Eng. **52**, 1 – 6 – 6 (2013).
7. S. Bloom, E. Korevaar, J. Schuster, and H. Willebrand, "Understanding the performance of free-space optics *[Invited]*," J. Opt. Netw. **2**, 178–200 (2003).
8. L. C. Andrews and R. L. Phillips, *Laser beam propagation through random media* (SPIE Press, 2005), II ed.
9. L. Li, T. Geng, Y. Wang, X. Li, J. Wu, Y. Li, S. Ma, S. Gao, and Z. Wu, "Free-space optical communication using coherent detection and double adaptive detection thresholds," IEEE Photon. J. **11**, 1–17 (2019).
10. S. Anees and M. R. Bhatnagar, "Performance of an amplify-and-forward dual-hop asymmetric RF-FSO communication system," IEEE/OSA J. Opt. Commun. Netw. **7**, 124–135 (2015).
11. M. Uysal and M. M. Faree, "Cooperative diversity systems for wireless communication," in *Sel. Topics in Inf. and Cod. Theo.*, (2010), pp. 623–662.
12. M. Safari and M. Uysal, "Relay-assisted free-space optical communication," IEEE Trans. Wirel. Commun. **7**, 5441–5449 (2008).
13. M. Karimi and M. Nasiri-Kenari, "BER analysis of cooperative systems in free-space optical networks," J. Light. Technol. **27**, 5639–5647 (2009).
14. C. K. Datsikas, K. P. Peppas, N. C. Sagias, and G. S. Tombras, "Serial free-space optical relaying communications over Gamma-Gamma atmospheric turbulence channels," IEEE/OSA J. Opt. Commun. Netw. **2**, 576–586 (2010).
15. M. R. Bhatnagar, "Performance analysis of decode-and-forward relaying in Gamma-Gamma fading channels," IEEE Photon. Technol. Lett. **24**, 545–547 (2012).
16. M. R. Bhatnagar, "Average BER analysis of differential modulation in DF cooperative communication system over Gamma-Gamma fading FSO links," IEEE Commun. Lett. **16**, 1228–1231 (2012).
17. M. Karimi and M. Nasiri-Kenari, "Free space optical communications via optical amplify-and-forward relaying," J. Light. Technol. **29**, 242–248 (2011).
18. S. Kazemlou, S. Hranilovic, and S. Kumar, "All-optical multihop free-space optical communication systems," J. Light. Technol. **29**, 2663–2669 (2011).
19. E. Bayaki, D. S. Michalopoulos, and R. Schober, "EDFA-based all-optical relaying in free-space optical systems," IEEE Trans. Commun **60**, 3797–3807 (2012).
20. M. A. Kashani, M. M. Rad, M. Safari, and M. Uysal, "All-optical amplify-and-forward relaying system for atmospheric channels," IEEE Commun. Lett **16**, 1684–1687 (2012).
21. P. V. Trinh, A. T. Pham, H. T. T. Pham, and N. T. Dang, "BER analysis of all-optical af dual-hop FSO systems over Gamma-Gamma channels," in *2013 IEEE 4th International Conference on Photonics (ICP),* (2013), pp. 175–177.
22. J. Libich, M. Komanec, S. Zvanovec, P. Pesek, W. O. Popoola, and Z. Ghassemlooy, "Experimental verification of an all-optical dual-hop 10 Gbit/s free-space optics link under turbulence regimes," Opt. Lett. **40**, 391–394 (2015).
23. N. A. M. Nor, Z. . Ghassemlooy, J. Bohata, P. Saxena, M. Komanec, S. Zvanovec, M. R. Bhatnagar, and M. Khalighi, "Experimental investigation of all-optical relay-assisted 10 Gb/s FSO link over the atmospheric turbulence channel," J. Light. Technol. **35**, 45–53 (2017).
24. N. A. M. Nor, J. Bohata, Z. Ghassemlooy, S. Zvanovec, P. Pesek, M. Komanec, J. Libich, and M. Khalighi, "10 Gbps all-optical relay-assisted fso system over a turbulence channel," in *2015 4th International Workshop on Optical Wireless Communications (IWOW),* (2015), pp. 69–72.
25. P. V. Mamyshev, "All-optical data regeneration based on self-phase modulation effect," in *24th European Conference on Optical Communication. ECOC '98 (IEEE Cat. No.98TH8398),* vol. 1 (1998), pp. 475–476 vol.1.
26. P. P. Baveja, D. N. Maywar, and G. P. Agrawal, "Optimization of all-optical 2R regenerators operating at 40 Gb/s: Role of dispersion," J. Light. Technol. **27**, 3831–3836 (2009).